The effect of normal electric fields on the Stokes drift

The effect of normal electric fields on the Stokes drift

Luiz P. Palacio[1], Marcelo V. Flamarion*,[2], Tao Gao[3], Roberto Ribeiro-Jr[1]

[1]UFPR/Federal University of Paraná, Departamento de Matemática, Centro Politécnico, Jardim das Américas, Caixa Postal 19081, Curitiba, PR, 81531-980, Brazil
[2]Departamento Ciencias-Sección Matemáticas, Pontificia Universidad Católica del Perú, Av. Universitaria 1801, San Miguel 15088, Lima, Peru
corresponding author*: mvellosoflamarionvasconcellos@pucp.edu.pe
[3]School of Mathematics, Statistics and Actuarial Science, University of Essex, Colchester CO4 3SQ, United Kingdom

Abstract

In periodic wave motion, particles beneath the wave undergo a drift in the direction of wave propagation, a phenomenon known as Stokes drift. While extensive research has been conducted on Stokes drift in water wave flows, its counterpart in electrohydrodynamic flows remains relatively unexplored. Addressing this gap, we investigate Stokes drift beneath periodic traveling irrotational waves on a dielectric fluid under the effect of normal electric fields. Through numerical simulations utilizing conformal mapping, we compute particle trajectories and analyze the resultant Stokes drift behaviors beneath periodic traveling waves. Our findings indicate that variations in the electric field impact particle velocities while maintaining trajectory shapes. Moreover, the kinetic energy associated with a particle depends on its depth location and is a non-decreasing convex function in a fixed frame and a constant in a moving frame, as observed in water wave flows.

1 Introduction

The study of particle trajectories beneath surface water wave dates back to 1839 with Stokes [46], whose results indicated that particles beneath a periodic wave undergo a drift in the direction of wave propagation, later called Stokes drift. In this way, he conjectured that particle paths are not closed.

The study of particle trajectories and Stokes drift is of significant physical and mathematical interest, with relevance to a wide range of applications. These include submarine operations and the transport of particles such as oil spills, gas bubbles, suspended sediment, and biological material. Moreover, Stokes drift contributes to the transport of heat, salt, and other natural or anthropogenic tracers, including microplastic pollution, in the upper ocean layer [3, 50].

The literature on Stokes drift and particle trajectories for water waves is vast and well established, including experimental investigations, numerical studies and rigorous mathematical analysis. Among the experimental works, we mention the findings of Longuet-Higgins [37], who determined the trajectory of a particle on the surface and found loop-shaped orbits with a drift in the direction of wave propagation. In addition, we refer to the work of Van den Bremer and Breivik [50], which provides a comprehensive review of the fluid mechanics of Stokes drift and its applications. A review of numerical strategies for computing particle trajectories is presented in [41], while additional details on Stokes drift and the characteristics of subsurface particle orbits beneath Stokes waves can be found in [40].

Constantin [8] rigorously proved Stokes' conjecture, demonstrating both the drift and the loop-shaped particle paths without any assumption of the depth regime. Constantin and Villari [9] obtained similar results for linear waves with a known velocity field. Two years later, Constantin and Strauss [10] showed that, in the presence of a uniform current, particles may in fact exhibit no drift.

More recently, significant progress has been made on particle trajectories beneath free-surface waves in reduced models [2, 5, 18, 19, 32]. For irrotational flows, Carter et al. [6] used the nonlinear Schrödinger equation to describe the surface of a Stokes wave and study the particle paths beneath it, obtaining results consistent with those for Stokes waves described by the Euler equations. Vanneste and Young [51] decomposed the Stokes drift into a solenoidal component and a remainder that is small for waves with slowly varying amplitudes, which simplifies the analysis of drift and trajectories. Abrashkin and Pelinovsky [1] analyzed Stokes drift beneath Stokes and Gerstner waves and showed a relation between them: the quadratic approximation of particle trajectories beneath a Stokes wave is a superposition of the vorticity flow of the Gerstner wave and the shear flow of Stokes drift. Weber [53] demonstrated that the Stokes drift beneath a Gerstner wave vanishes using a nonlinear Lagrangian formulation.

Stokes drift can be observed not only in surface gravity waves but also in other types of waves, such as vertically confined internal modes, oceanic Kelvin and Rossby waves, or acoustic waves (see [50] and references therein). In this paper we focus on Stokes drift beneath a Stokes wave in electrohydrodynamic (EHD) flows. A Stokes wave is a periodic traveling wave with a symmetric profile that rises and falls exactly once per wavelength.

Electrohydrodynamics (EHD) is a topic of study that examines the coupling between the motion of charged fluids and electric fields, with particular attention to interfaces between fluids, which arise frequently in practical applications. EHD has numerous applications in chemical engineering, for example, in coating processes [33, 27], cooling systems for high-power devices [24], and electrospray technology [48], due to the relative ease with which fluid flows can be manipulated artificially. A natural question that arises is how an electric field might influence the phenomenon of Stokes drift. To provide a broader context and intuition, we therefore include a brief review of electrohydrodynamic flows and wave motion. The readers may also refer to [7, 43] for

more details. There were two major early achievements in the literature on interfacial waves by Taylor & McEwan [47] and Melcher & Schwarz [38] respectively. The former work theoretically and experimentally demonstrated that the interface between a conducting fluid and a dielectric could be destabilized due to normal electric fields perpendicular to the undisturbed interface (i.e. vertically). Meanwhile, the latter work considered the problem with tangential electric fields parallel to the undisturbed surface and showed by performing a linear stability analysis that short waves could be regularised under this setting. Since then, many authors have continued to investigate the role of electric fields in (de)stabilizing various interfacial fluid configurations [39]. For the problem of vertical electric fields, the most general setting concerns two immiscible fluids, with an interface in between, of perfect dielectric of different electric permittivities (see [13] for details). Some assumptions are usually made to simplify the problem. One common setup is to consider the upper layer to be a hydrodynamically passive region of dielectric and the lower layer to be a conducting fluid, see e.g. [44, 16, 42, 25, 30, 31, 14]. The other common assumption is to let the upper layer be conducting gas while the lower layer is a dielectric fluid, which reduces the physical configuration to a one-layered problem, see e.g. [22, 23, 17, 21]. A direct question in the present context is how electric fields affect the Stokes drift. To fill this gap in the literature, we investigate the Stokes drift of a charged particle beneath an irrotational Stokes wave under normal electric fields in the same one-layered physical configuration in this paper. The two major physical assumptions (inviscid fluid and perfectly conducting gas) are justified as follows. The viscous effect on wave drift is most pronounced near boundaries and has a limited impact on the bulk fluid, as demonstrated by Longuet-Higgins [35]. Since this study does not focus on boundary layers, the fluid is assumed to be inviscid. For investigations near boundaries, viscous effects cannot be neglected. On the other hand, the primary objective of this study is to investigate the electric effect on Stokes drift. To achieve this, it is necessary to establish a significant contrast in permittivities between the two layers, as in chemical engineering; otherwise, the electrohydrodynamic effects are minimal. Such a consideration motivates the assumption that the gas layer is perfectly conducting.

We highlight that, although the modeling equations used in this work are the same as in [17], the phenomena under investigation differ. That reference focuses on the flow structure beneath nonlinear periodic waves in the presence of a linearly sheared current, introducing a constant vorticity as an additional parameter in the dynamical system for particle trajectories and motivating a bifurcation analysis with respect to this parameter. By contrast, the flow considered here is irrotational, and our interest lies in Stokes drift: particles beneath the wave experience a net drift in the direction of wave propagation.

In this article, we use conformal mapping and pseudo-spectral numerical methods to compute particle trajectories and evaluate Stokes drift. The rest of the work is structured as follows: The mathematical formulation is presented in Section 2. The linear case and the properties of Stokes drift are reviewed in Section 3. The numerical method for the nonlinear problem is given in Section 4. Results are presented in

Section 5, and concluding remarks are provided in Section 6.

2 Mathematical Formulation

We consider an inviscid and incompressible dielectric fluid of permittivity ϵ_0 bounded by wall electrodes on top and bottom, imposed with a constant voltage difference inbetween, and surrounded by a conducting gas. In this case, the fluid is conditioned to the action of a normal electric field ($\vec{E} = \nabla V$), in which V is a voltage potential. We may let $V = 0$ on top and $V = -V_0$ on bottom without losing generality.

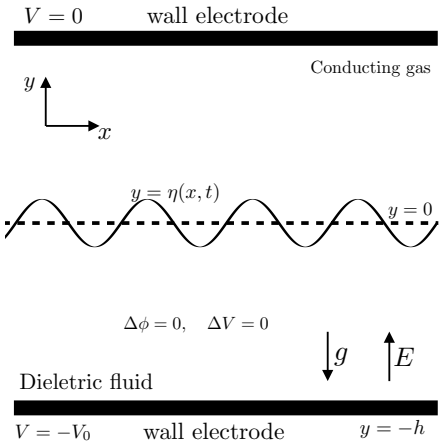

Figure 1: Sketch illustrating the physical context of the problem.

Let $\vec{U} = \nabla\phi$ represent the irrotational velocity field of the fluid motion, where ϕ is a velocity potential. We denote the fluid surface by $\eta(x,t)$ which is assumed to be a traveling wave with phase speed c. The functions $\eta(x,t)$ and $\phi(x,y,t)$ are assumed to be λ-periodic in the x variable and of the form $\eta(x,t) = \eta(x-ct)$ and $\phi(x,t) = \phi(x-ct,y)$ A schematic is depicted in Figure 1. By introducing the change of variables $X = x - ct$ and $Y = y$, we can express the fluid surface as $\eta(x,t) = \eta(X)$. Then, following the approach in [17], we can express the Euler governing equations in dimensionless form by selecting h, $\sqrt{h/g}$ and V_0 as the reference length, time and voltage potential, in terms of the electric field and velocity potentials as follows

$$\Delta\phi = 0 \quad \text{in} \quad -1 < Y < \eta(X), \tag{1}$$
$$\Delta V = 0 \quad \text{in} \quad -1 < Y < \eta(X), \tag{2}$$
$$-c\eta_X + \phi_X\eta_X = \phi_Y \quad \text{for} \quad Y = \eta(X), \tag{3}$$
$$\phi_Y = 0 \quad \text{for} \quad Y = -1, \tag{4}$$
$$V = 0 \quad \text{for} \quad Y = \eta(X), \tag{5}$$
$$V = -1 \quad \text{for} \quad Y = -1. \tag{6}$$

In addition to governing equations, we have the dynamic boundary condition:

$$-c\phi_X + \frac{1}{2}(\phi_X^2 + \phi_Y^2) + \eta + M_e = B, \tag{7}$$

where B is the Bernoulli constant and M_e represents the Maxwell stress tensor given by

$$M_e = \frac{E_b}{2(1+\eta_X^2)}\Big[(1-\eta_X^2)(V_Y^2 - V_X^2) - 4\eta_X V_X V_Y\Big] = \frac{E_b}{2}|\nabla V|^2. \tag{8}$$

The parameter E_b represent the nondimensional Electric Bond number defined as follows

$$E_b = \frac{\epsilon_0 V_0^2}{\rho g h^3}, \tag{9}$$

where ρ denote the density of the dielectric fluid and g the gravitational acceleration.

In the wave-moving frame, the trajectory $(X(t), Y(t))$ of a fluid particle in the dielectric fluid is governed by the dynamical system

$$\begin{cases} \dfrac{dX}{dt} &= \phi_X(X,Y) - c, \\ \dfrac{dY}{dt} &= \phi_Y(X,Y). \end{cases} \tag{10}$$

In this frame, the trajectory coincides with the streamline of the flow.

The system (10) can be easily obtained by noting that if (x_0, y_0) is the initial position of a particle in the fixed frame (x, y), where the wave moves to the left or right at a constant velocity, its trajectory $(x(t), y(t))$, $t \geq 0$, is obtained as the solution of

$$\begin{cases} x'(t) = \phi_x(x - ct, y), \\ y'(t) = \phi_y(x - ct, y), \end{cases} \quad \text{with initial data } (x(0), y(0)) = (x_0, y_0). \tag{11}$$

Thus, the trajectory $(x(t), y(t))$ in the fixed coordinates (x, y) corresponds to the trajectory $(X(t), Y(t))$ in the wave–moving frame coordinates, given by

$$X(t) = x(t) - ct, \quad Y(t) = y(t),$$

where $(X(t), Y(t))$ is the solution of (10).

2.1 Stokes Drift

In this section, we recall some properties and results on Stokes drift for water waves that are known in the literature.

For a solution $(X(t), Y(t))$ of the ODE system (10) with the initial condition (X_0, Y_0), where $Y_0 \in [-1, \eta(X_0)]$, the time required for this solution to travel a single wavelength, i.e. reach $X = X_0 - \lambda$, is called the drift time and is denoted by $\tau(Y_0)$. This represents the time that a particle takes to traverse one period in the moving frame. The drift time can also be interpreted as the Lagrangian period, that is, the time for a particle to return to its original height in the fluid [28].

Constantin [8] proved the following formula to calculate the drift time of a particle trajectory

$$\tau(Y_0) = \int_{-\lambda/2}^{\lambda/2} \frac{dX}{c - \phi_X(X, Y_0)} \tag{12}$$

Furthermore, Li and Yang [34] has shown that the drift time must satisfy the following inequality

$$\frac{\lambda}{c} < \tau(Y_0) \leq \int_{-\lambda/2}^{\lambda/2} \frac{1}{c - \phi_X(X, \eta(X))} dx, \tag{13}$$

where λ/c is the Eulerian wave period.

Following the established notation, we define the Stokes Drift as the distance between the points $(x(0), y(0))$ and $(x(\tau(Y_0)), y(\tau(Y_0)))$, where $x(t) = X(t) + ct$ and $y(t) = Y(t)$. As we can see at Li and Yang [34], a direct implication from (13) is that the Stokes Drift is always positive. It is important to note, however, that this conclusion holds only for perfectly periodic waves with a zero mean free-surface level. In realistic scenarios (whether in laboratory or oceanic conditions) the Stokes drift may exhibit both positive and negative values due to the influence of boundary layers [28] or the presence of a non-zero mean surface elevation, which is common under natural ocean conditions [4, 29].

In our upcoming numerical experiments, we will investigate the properties of Stokes drift in the context of EHD flows. Additionally, we aim to analyze certain geometric characteristics of particle trajectories. To achieve this, we introduce the following three parameters:

1. d_1 is the Stokes drift of the trajectory;

2. d_2 is the horizontal distance between the leftmost and rightmost points of the trajectory, defined $d_2 = x(t_2) - x(t_1)$, where $x(t_1) = \min_{t \in [0, \tau(Y_0)]} x(t)$ and $x(t_2) = \max_{t \in [0, \tau(Y_0)]} x(t)$.

3. d_3 is the vertical distance between the lowest and highest points of the trajectory, defined as is the distance between $d_3 = y(t_4) - y(t_3)$, where $y(t_3) = \min_{t \in [0, \tau(Y_0)]} y(t)$ and $y(t_4) = \max_{t \in [0, \tau(Y_0)]} y(t)$.

Figure 2 presents a schematic representation of the parameters d_1, d_2, and d_3.

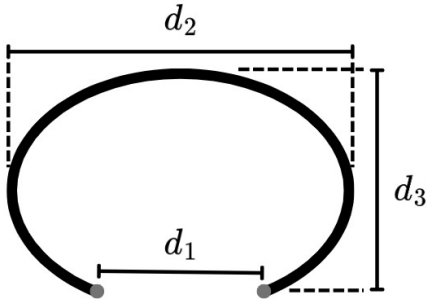

Figure 2: Geometric parameters indicating the aspect ratio of a trajectory.

3 Linear theory

In this section, we present the linear theory to derive an explicit formula for the velocity field of the dynamical system (10).

A trivial solution for the governing equations (1)-(7) is

$$\begin{cases} \bar{\eta}_0(X) = 0, \\ \bar{\phi}_0(X,Y) = 0, \\ \bar{V}_0(X,Y) = Y, \end{cases}$$

which is perturbed by a small disturbance measured by a parameter ε ($\ll 1$), namely

$$\begin{cases} \eta(X) = \varepsilon\hat{\eta}, \\ \phi(X,Y) = \varepsilon\hat{\phi}, \\ V(X,Y) = Y + \varepsilon\hat{V}. \end{cases}$$

Here, ε is a small parameter that measures the wave amplitude. Solving Laplace equations with boundary conditions as described in (1)-(7) yields

$$\begin{cases} \hat{\eta}(X) = \Re\{Ae^{ikX}\}, \\ \hat{\phi}(X,Y) = \Re\{Be^{ikX}\cosh(k(Y+1))\}, \\ \hat{V}(X,Y) = \Re\{Me^{ikX}\sinh(k(Y+1))\}. \end{cases} \tag{14}$$

Here, A, B, and M are unknown constants, and $k = 2\pi/\lambda$ is the wavenumber. By linearizing the dynamic and kinematic boundary conditions, we obtain

$$\begin{cases} B = \frac{-iAc}{\sinh(k)}, \\ M = \frac{-A}{\sinh(k)}, \end{cases}$$

the linear speed

$$c^2 = \frac{\tanh(k)}{k} - E_b, \tag{15}$$

and the linear velocity field

$$\hat{\phi}_X(X,Y) = \frac{kAc\cos(kX)\cosh(k(Y+1))}{\sinh(k)}, \tag{16}$$

$$\hat{\phi}_Y(X,Y) = \frac{kAc\sin(kX)\sinh(k(Y+1))}{\sinh(k)}. \tag{17}$$

From this point on, we only consider the positive value of c, i.e., the right moving waves. Note that there exists a critical value E_b^* such that waves are destabilized by the electric field when $E_b > E_b^*$ as the wave speed no longer admits a real solution. In the particular case $\lambda = 2\pi$ (i.e., $k = 1$), we have $E_b^* = \tanh(1)$. To obtain a more accurate description of the limiting behavior of τ, which tends to infinity as $E_b \to E_b^*$, a nonlinear theory is required.

4 The nonlinear problem: conformal mapping and numerical method

To solve the dynamical system (10), we consider the velocity field solution of the full nonlinear Euler equations (1)-(7) by employing the conformal mapping formulation presented in [17], combined with the trajectory computation strategy outlined in [45]. These approaches are based on the conformal mapping introduced by [15], which provided the foundation for the development of pseudospectral numerical methods for free-surface hydrodynamic problems in various contexts.

The numerical methodology applied in our study consists of three main steps:

1. Construct the conformal mapping suitable for the problem.
2. Reformulate the Euler equations (1)-(7) in canonical coordinates. This reformulation allows us to determine a free-surface wave solution and the velocity field in the fluid domain for a given E_b.
3. Solve the dynamical system (10) in canonical coordinates, then map the corresponding trajectory back to the physical domain.

For further details, we refer the reader to [17] and [45]. Here, we summarize only the key aspects of each step.

1) Construct the conformal mapping suitable for the problem

First, we construct a conformal mapping

$$Z(\xi,\zeta) = \tilde{X}(\xi,\zeta) + i\tilde{Y}(\xi,\zeta),$$

which maps the strip of width D and length L,

$$\{(\xi,\zeta) \in \mathbb{R}^2 \mid -\frac{L}{2} < \xi < \frac{L}{2}, -D < \zeta < 0\},$$

onto the physical domain of a wavelength λ,

$$\{(X,Y) \in \mathbb{R}^2 \mid -\frac{\lambda}{2} < X < \frac{\lambda}{2}, -1 < Y < \eta(X)\}.$$

This mapping flattens the free surface and satisfies the boundary conditions

$$\tilde{Y}(\xi,0) = \eta(\tilde{X}(\xi,0)), \quad \text{and} \quad \tilde{Y}(\xi,-D) = -1.$$

Using algebraic manipulations, the Fourier transform, and the assumption that Z is conformal, we obtain the following expressions:

$$\tilde{X}(\xi,\zeta) = -\mathcal{F}^{-1}_{k_j\neq 0}\left[\frac{i\cosh(k_j(D+\zeta))}{\sinh(k_jD)}\mathcal{F}[\mathbf{Y}](k_j)\right] + \xi, \tag{18}$$

$$\tilde{Y}(\xi,\zeta) = \mathcal{F}^{-1}_{k_j\neq 0}\left[\frac{\sinh(k_j(D+\zeta))}{\sinh(k_jD)}\mathcal{F}[\mathbf{Y}](k_j)\right] + \frac{\hat{\mathbf{Y}}(0)+1}{D}\zeta + \hat{\mathbf{Y}}(0). \tag{19}$$

where $\mathbf{Y}(\xi) = \eta(\tilde{X}(\xi,0))$ and $\mathcal{F}[\cdot]$ denotes the Fourier transform:

- $\mathcal{F}[f(\xi)] = \hat{f}(k_j) = \frac{1}{L}\int_{-L/2}^{L/2} f(\xi)e^{-ik_j\xi}\,d\xi$;
- $\mathcal{F}^{-1}[\hat{f}(k_j)] = f(\xi) = \sum_{j\in\mathbb{Z}} \hat{f}(k_j)e^{ik_j\xi}$;

where $k_j = \frac{2\pi}{L}j$.

2) Reformulating the Euler equations in canonical coordinates.

We impose that the free surface has the same wavelength in both coordinate systems, i.e., $L = \lambda$. This condition leads to the relation:

$$D = \frac{1}{L}\int_{-L/2}^{L/2} \mathbf{Y}(\xi)\,d\xi + 1. \tag{20}$$

Let ψ be the harmonic conjugate of ϕ, and define

$$\tilde{\phi}(\xi,\zeta) = \phi(\tilde{X}(\xi,\zeta),\tilde{Y}(\xi,\zeta)), \quad \tilde{\psi}(\xi,\zeta) = \psi(\tilde{X}(\xi,\zeta),\tilde{Y}(\xi,\zeta)).$$

Denoting $\mathbf{X}(\xi)$ as the horizontal component of the conformal map evaluated at $\zeta = 0$, the free surface in the canonical coordinate system corresponds to the curve $(\mathbf{X}(\xi),\mathbf{Y}(\xi))$. The kinematic (3) and Bernoulli (7) conditions reduce to:

$$\frac{-c^2}{2} + \frac{c^2}{2\mathbf{J}} + \mathbf{Y} + \frac{E_b}{2D^2\mathbf{J}} - B = 0, \tag{21}$$

where $\mathbf{J} = \mathbf{X}_\xi^2 + \mathbf{Y}_\xi^2$ is the Jacobian of the mapping evaluated at $\zeta = 0$. We can rewrite Equation (21) as

$$\frac{1}{2}\Big(\frac{1}{\mathbf{J}} - 1\Big)\Big(c^2 + \frac{E_b}{D^2}\Big) + \mathbf{Y} - B = 0. \tag{22}$$

It is noted that there is a term in $\frac{E_b}{2D^2}$, which has been absorbed into the Bernoulli constant B. In this way, for any electrified periodic wave solution with profile $\mathbf{Y}$ (D the associated depth in the canonical plane) and speed c in the presence of electric fields of strength E_b, the wave profile must be the same as a classic Stokes wave with speed c_s where

$$c_s^2 = c^2 + \frac{E_b}{D^2}\,. \tag{23}$$

Increasing the electric Bond number (E_b) would lead to a decrease in the value of the wave speed.

Equation (21) involves four unknowns: $\mathbf{Y}$, c, B, and D. To complete the system, we impose three additional conditions:

1. Fixed wave height:
$$\mathbf{Y}(0) - \mathbf{Y}(L/2) = H. \tag{24}$$

2. Zero-mean wave profile in the physical space:
$$\int_{-L/2}^{0} \mathbf{Y}\mathbf{X}_\xi \, d\xi = 0. \tag{25}$$

3. Depth condition (20).

The equations (21), (24), (25), and (20) are discretized spectrally, with derivatives computed via the Fast Fourier Transform (FFT) and integrals approximated using the trapezoidal rule. The periodicity of the wave motion is automatically guaranteed under this scheme, as is the mass conservation. The resulting system is solved numerically using Newton's continuation method. All calculations employ 1024 Fourier modes, with $L = 2\pi$.

3) Solve the dynamical system (10) *in canonical coordinates, then map the corresponding trajectory back to the physical domain.*

The trajectory $(X(t), Y(t))$, which is the solution of the ODE system (10), corresponds to the image of a trajectory $(\xi(t), \zeta(t))$ in the canonical domain under the conformal mapping. Specifically, we have
$$(X(t), Y(t)) = (\tilde{X}(\xi(t), \zeta(t)), \tilde{Y}(\xi(t), \zeta(t))), \tag{26}$$
where $(\xi(t), \zeta(t))$ is determined by the system
$$\begin{cases} \dfrac{d\xi}{dt} &= \dfrac{1}{J}\left(\tilde{\phi}_\xi - c\tilde{Y}_\zeta\right), \\ \dfrac{d\zeta}{dt} &= \dfrac{1}{J}\left(\tilde{\phi}_\zeta + c\tilde{Y}_\xi\right). \end{cases} \tag{27}$$
where $J(\xi, \zeta) = \tilde{X}_\xi^2 + \tilde{Y}_\xi^2$ is the Jacobian and the velocity potential $\tilde{\phi}(\xi, \zeta)$ is given by
$$\tilde{\phi}(\xi, \zeta) = \mathcal{F}_{k\neq 0}^{-1}\left[\frac{\cosh(k_j(D+\zeta))}{\cosh(k_j D)}\hat{\mathbf{\Phi}}(k_j)\right], \tag{28}$$
with $\mathbf{\Phi} = -\mathcal{C}[\mathbf{\Psi}]$, where the operator $\mathcal{C}[\cdot]$ is defined as $\mathcal{C}[\cdot] := \mathcal{F}^{-1}[i\coth(k_j D)\mathcal{F}[\cdot]]$. Additionally, the stream function satisfies $\mathbf{\Psi} = c\mathbf{Y}$.

Particle trajectories are computed numerically by integrating (27) in the canonical domain usinglab the fourth-order Runge-Kutta method. The resulting trajectories

are then mapped onto the physical domain, yielding the trajectory $(X(t), Y(t))$ in the moving frame. To analyze the particle paths in the fixed frame, we apply the transformation

$$x(t) = X(t) + ct, \quad y(t) = Y(t).$$

Furthermore, as mentioned at the beginning of Section 2.1, the drift time is obtained numerically by determining the time required for a particle, initially located at (X_0, Y_0) with $Y_0 \in [-1, \eta(X_0)]$, to travel one wavelength in the fixed frame, that is, to reach $X = X_0 - \lambda$. This computation is performed using equation (27) for nonlinear waves and equation (10), with the velocity field derived from the linear theory, for linear waves.

5 Numerical results

In this section, we present the results of numerical experiments for various electric Bond numbers (E_b).The objective is to understand the electric effect in the Stokes drift.

We fix the depth at 1, and set the wavelength (λ) to 2π. We focus on this intermediate-depth regime and control the wave profile through the steepness parameter $s = H/\lambda$. We conduct a similar work for waves in shallow-water regime $\lambda = 20\pi$ and deep-water regime ($\lambda = 0.2\pi$) in Appendix A.

It is noted that, based on the linear wave speed from (15), again with this set of parameters, the electric Bond number E_b must satisfy $E_b \leq E_b^*$ such that c admits a real solution, in which $E_b^* = \tanh 1$ is the critical value as previously introduced.

5.1 Particle trajectories and Stokes drift

In this subsection, we explore the geometric parameters of the particle path, drift time, and wave speed for various values of E_b. Unless stated otherwise, the free-surface wave is fixed with a steepness of $s = 0.09$ that guarantees us a strongly nonlinear wave profile with height $H \approx 0.5655$. Similar to a remark made by [22] for the case of infinite depth, two electrified solutions may share the same wave profile as long as

$$c_1^2 + \frac{E_{b1}}{D_1^2} = c_2^2 + \frac{E_{b2}}{D_2^2}\,, \tag{29}$$

due to equation (22) and (23). The value of the depth in the canonical domain does not vary provided the surface displacement is unchanged, and therefore, the main response to a change in E_b may be reflected in the wave speed. This is confirmed by our numerical computations for three different values of E_b as shown in Figure 3, where the wave profiles for a fixed steepness look identical and the associated wave speed decreases as E_b increases. To further support this observation, we evaluated the pairwise distances $\|\mathbf{Y}_i - \mathbf{Y}_j\|_2$ between the solutions shown in Figure 3. The

computed distances are of the order of 10^{-15}, which is comparable to numerical error. The numerical evidence shows that these three wave profiles are identical, and the difference is only subject to numerical error.

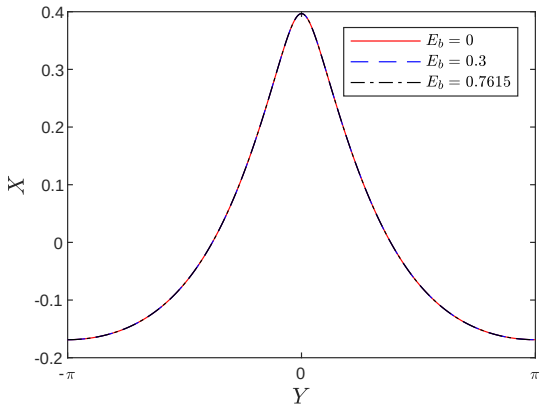

Figure 3: Wave profile for different values of E_b for a fixed steepness $s = 0.09$.

The dynamical system (10) is solved with the initial condition beneath the trough at (π, Y_0). Figure 4 displays the trajectory of a particle starting from initial position $(\pi, -0.5627)$, $Y_0 \approx -0.5627$ corresponds to a depth of $\zeta = -D/2$ in the canonical domain, for the cases where $E_b = 0$, 0.3, and 0.7615. We observe that higher values of E_b result in slower particle motion. The dependence of the drift time on E_b is examined in Figure 5.

The left graph in Figure 5 shows the wave speed (c), while the right graph shows the drift time (τ) for various values of E_b. The particle's initial depth is $Y_0 \approx -0.5627$, which corresponds to a depth of $\zeta = -D/2$ in the canonical domain. For the linear solution, $Y_0 = -0.5$ (corresponding to $(\xi_0, \zeta_0) = (\pi, -D/2)$) and the trajectories are computed explicitly using linear theory. Note that, while the variation of E_b does not affect the wave profile, the particle initial depth Y_0 remains identical regardless of E_b value. We observe that increasing E_b leads to a decrease in wave speed and an increase in drift time. Additionally, Figure 6 shows that the drift time is larger near the free surface and decreases as we move from the trough toward the bottom, a result previously established for for $E_b = 0$ [34] and still valid for $E_b \neq 0$.

We recall the inequality (13), which holds for water wave flow when $E_b = 0$. This inequality establishes lower and upper bounds for the drift time of a particle initially located at depth Y_0. As shown previously, when an electric field is introduced, the drift time also depends on the field intensity E_b. A natural question then arises: does inequality (13) still hold when $E_b \neq 0$?

To address this question, we computed $\tau(Y_0)$ under two distinct conditions: (i) by fixing $Y_0 = -0.5627$ and varying E_b; and (ii) by fixing $E_b = 0.7$ and varying Y_0. The corresponding results are presented in Figure 7. In the left panel, where Y_0 is fixed and E_b varies, we observe that the drift time $\tau(Y_0)$ remains bounded, consistent with the prediction of inequality (13). The right panel displays the variation of $\tau(Y_0)$ with depth for a fixed electric Bond number $E_b = 0.7$, suggesting that inequality (13) may

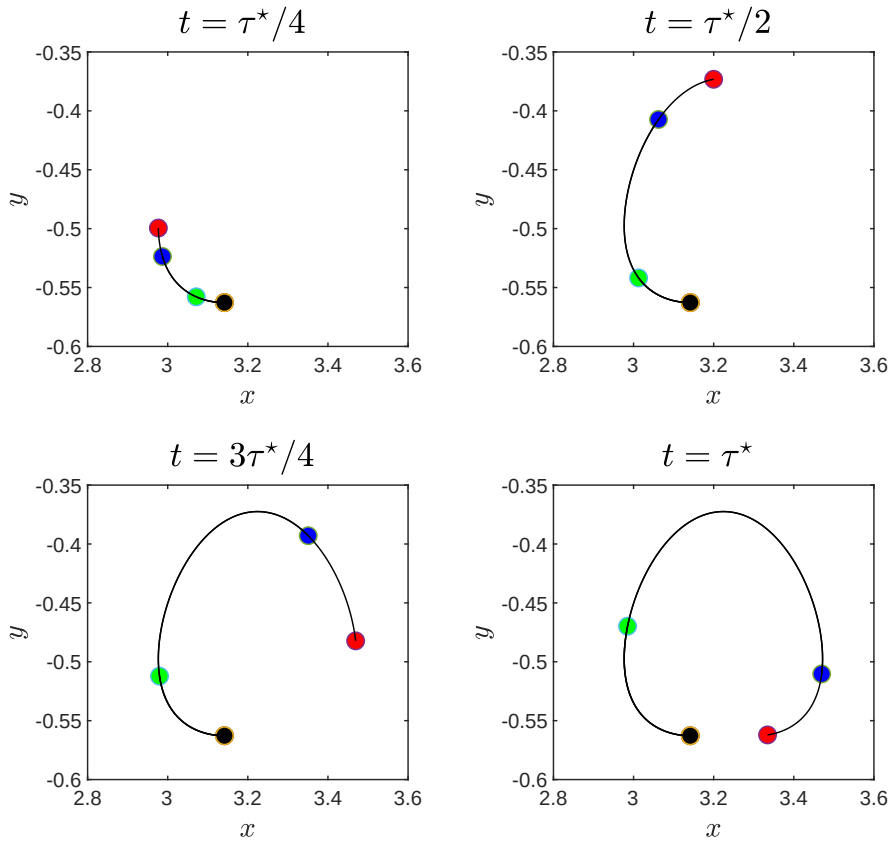

Figure 4: Snapshots of the trajectory of a particle starting from the same initial position, $(\pi, -0.5627)$, for the cases where $E_b = 0$ (red), 0.3 (blue), and 0.7615 (green). $\tau^\star$ represents the drift time of the particle for $E_b = 0$ and black dot the initial position of the particle.

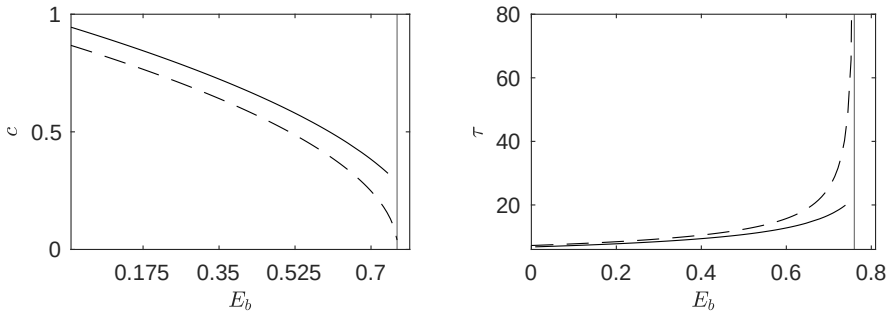

Figure 5: Speed (c) and drift time (τ) as functions of the electric Bond number (E_b). Results are shown for the linear theory (dashed lines) and the nonlinear theory (solid lines). Vertical lines indicate the critical value of E_b predicted by the linear theory ($\tanh 1$).

also hold in this electrified setting. In addition, although not shown in the the text to avoid repetition, we performed an additional numerical simulation for the limit case $E_b = 0.76159 \approx \tanh(1)$. These simulations indicate that as $E_b \to E_b^*$, the lower bound of inequality (13) increases, while the inequality itself remains valid.

To analyze the geometric parameters (d_1, d_2, d_3) of the particle trajectories, we first compute their values for the case $E_b = 0$, denoted as $(d_1^\star, d_2^\star, d_3^\star)$, and use them as a reference to compare the results for other values of E_b. The parameters d_i were

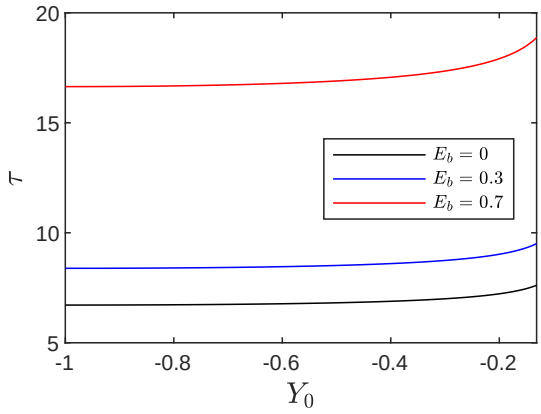

Figure 6: Drift time as a function of Y_0 for various values of E_b.

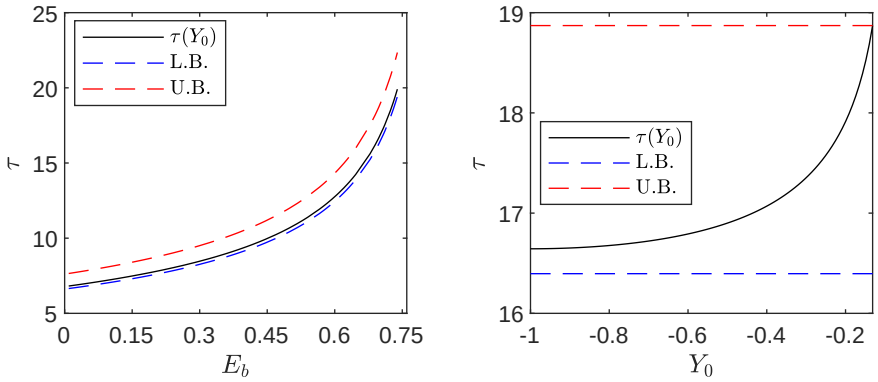

Figure 7: Comparison between the upper (UB) and lower (LB) bounds of inequality (13), originally established for water waves, and their counterparts in electrohydrodynamic (EHD) flows. Left: variation of the drift time $\tau(Y_0)$ with the electric Bond number E_b for a fixed initial depth $Y_0 = -0.5627$. Right: variation of $\tau(Y_0)$ with depth for a fixed electric Bond number $E_b = 0.7$.

computed for a particle initially located at $(\pi, -0.5627)$, where $Y_0 \approx -0.5627$ corresponds to a depth of $\zeta = -D/2$ in the canonical domain. The relative deviation of the trajectory parameters with respect to the reference case $E_b = 0$ is defined as

$$E_r(d_i) = \frac{|d_i - d_i^\star|}{|d_i^\star|}, \quad i = 1, 2, 3.$$

As shown in Figure 8, the relative deviation of the geometric parameters d_1, d_2, and d_3 remain small, which suggests that the trajectory shape is largely preserved as E_b increases, although the particle motion slows down. This can be explained by noting that in the canonical domain, the velocity field of ODE (27) can be written as a component that is independent of E_b, multiplied by the wave speed c. Therefore, variations in E_b only rescale c, leaving the particle paths unchanged while modifying only the parametrization speed along them. For completeness, a detailed derivation of this result is provided in Appendix B.

In summary, Figure 9 highlights the main results of this section and illustrates again that E_b affects only the parametrization of the particle trajectories. The figure also

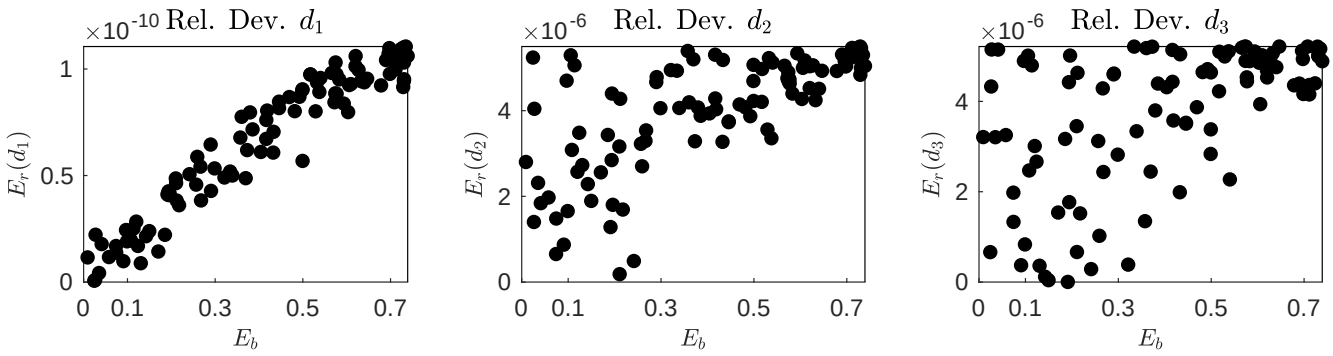

Figure 8: Relative deviation of the trajectory parameters d_1 (left), d_2 (center), and d_3 (right) with respect to the reference case $E_b = 0$, as a function of E_b.

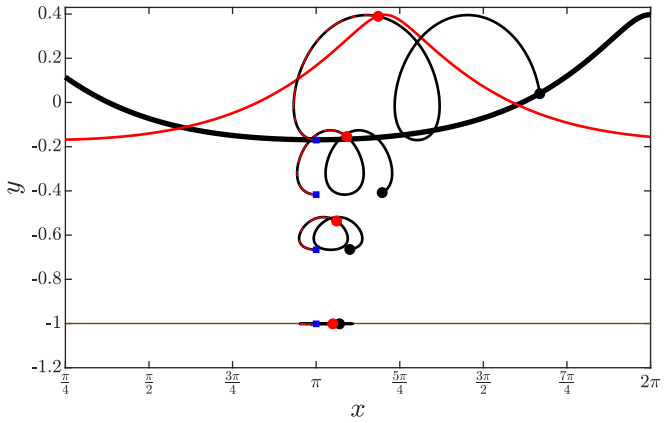

Figure 9: Red solid line: free surface wave for $E_b = 0.76$; black solid line: free surface wave for $E_b = 0$; thin brown solid line: bottom at $y = -1$. Particle trajectories beneath the free-surface wave are shown for $E_b = 0$ (black) and $E_b = 0.76$ (red). At $t = 0$, all particles are positioned at $x_0 = \pi$ and at the indicated depth y_0. These initial points are marked as blue squares. Trajectories within the fluid body form rightward loops, while the one at the bottom display back-and-forth motion.

shows that the particle drift is largest at the free surface and decreases with depth. Particles located at the bottom exhibit a back-and-forth motion: initially moving to the left, then turning to the right, and finally returning to the left, with their net displacement after one period ending to the right of $(\pi, -1)$. Moreover, since that our numerical simulation indicates that E_b only affects the parametrization of the trajectories, the known decay of the geometric parameters d_1, d_2, and d_3 with depth, established for classical water waves [40], are expected to remain valid in the context of EHD flow.

5.2 On the kinetic energy

The total kinetic energy of a fluid particle initially located at (X_0, Y_0) over a drift time in the moving frame is given by

$$E(X_0, Y_0) = \int_0^{\tau(Y_0)} \left[\left(\frac{dX}{dt} \right)^2 + \left(\frac{dY}{dt} \right)^2 \right] dt. \tag{30}$$

By changing to the fixed frame, where $X = x - ct$ and $Y = y$, the total kinetic energy over a drift time period in this frame is

$$\mathcal{E}(X_0, Y_0) = \int_0^{\tau(Y_0)} \left[\left(\frac{dX}{dt} + c \right)^2 + \left(\frac{dY}{dt} \right)^2 \right] dt. \tag{31}$$

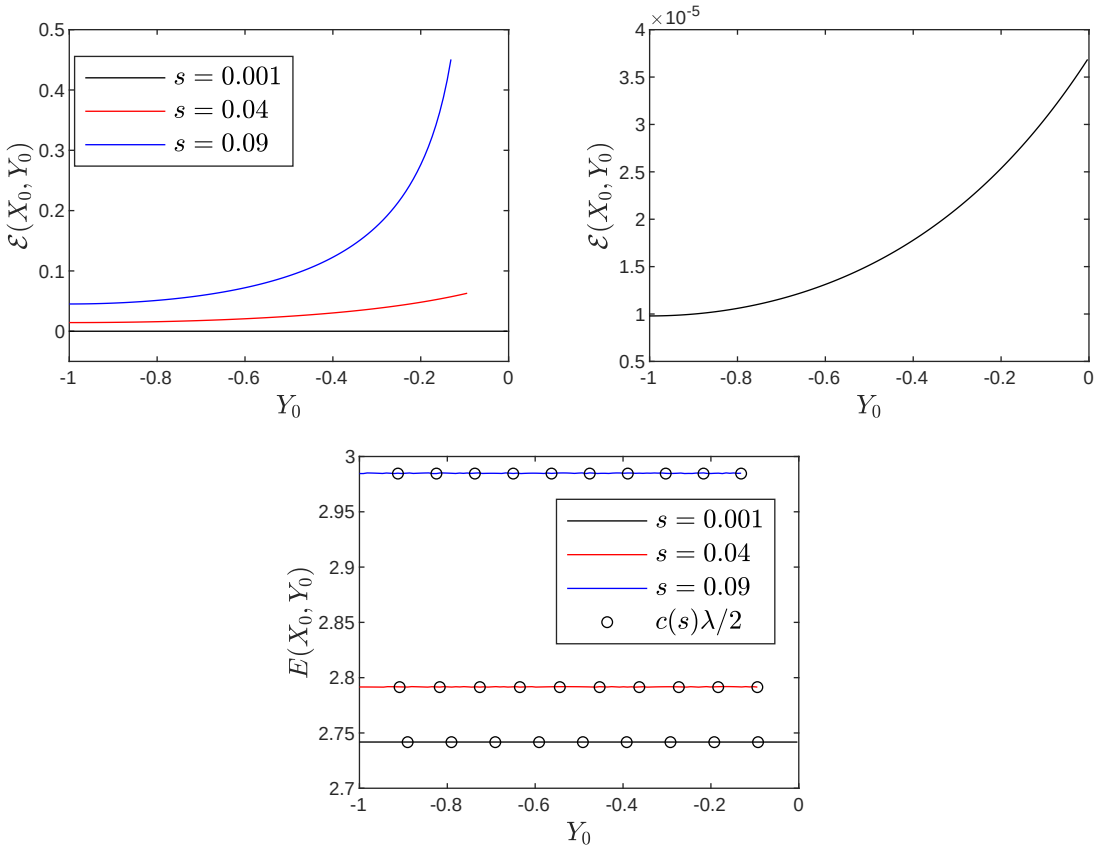

Figure 10: Top-left: Kinetic energy in the fixed frame for various wave steepness values as a function of the particle's initial depth (Y_0). Top-right: a zoomed-in graph for $s = 0.001$. Bottom: Kinetic energy in the moving frame.

For water wave flows, it is known that [11, 12, 34]:

1. $E(X_0, Y_0)$ is a constant given by $c\lambda/2$.
2. $\mathcal{E}(X_0, Y_0)$ is a convex, non-decreasing function that depends solely on Y_0.

In the absence of an electric field, decreasing the wave steepness results in smaller kinetic energy as shown in Figure 10. For $s = 0.001$, $\mathcal{E}$ is significantly lower than in the other cases, warranting a zoomed-in figure for clarity. Moreover, Figure 10 (bottom) illustrates that our numerical approach reproduces well the result known for water waves, namely $E(X_0, Y_0) = c\lambda/2$.

In addition, we want to numerically confirm the physical intuition that a decrease in steepness s leads to lower kinetic energy in the context of EHD flows. To this end, we compute the total kinetic energy of 100 simulations, each corresponding to a particle initially located at $X_0 = \pi$ with a distinct value of 0 Y_0 uniformly sampled within the interval $[-1, \eta(X_0)]$. Figure 11 illustrates that varying E_b ($E_b = 0, 0.3, 0.7$) preserves the known kinetic energy properties of water wave flows. Increasing E_b leads to a decrease in kinetic energy in both frames.

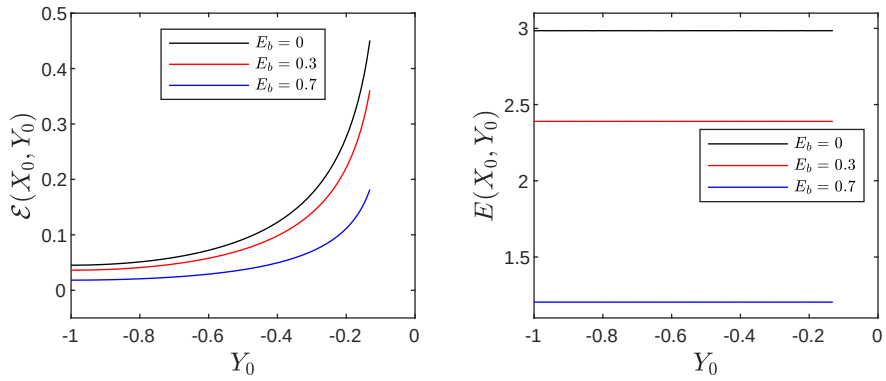

Figure 11: Kinetic energy in the fixed frame (left) and the moving frame (right) as a function of the particle's initial depth (Y_0) for different values of E_b.

6 Discussion

In this work, we investigated the influence of the electric Bond number (E_b) on the Stokes Drift of a particle beneath a Stokes wave. Our numerical experiments indicate that increasing E_b reduces wave speed and increases drift time. Additionally, the electric field slows down the particle trajectory while preserving its shape. Further, numerical results indicate that: (i) the inequality (13), and (ii) the property that drift time is larger near the free surface and decreases with increasing depth, both originally established for water waves, remain valid for EHD flows.

We also examined the kinetic energy properties of particle trajectories under periodic waves within the EHD flow framework. Our results indicate that kinetic energy is a non-decreasing convex function in the fixed frame and remains constant in the moving frame, as its behaviour in water wave flows without an electric field.

Beyond these specific findings, our study highlights a broader implication: for the physical configuration considered here, the electric field influences the system solely through its effect on the wave speed. This feature may prove advantageous in engineering applications where wave retardation is desirable, for instance in scenarios requiring

controlled particle transport or reduced mixing. The situation may, however, be different in the converse configuration, where the fluid layer is perfectly conducting and the gas layer is dielectric. In that case, the electric field may alter not only the wave speed but also the geometry of particle trajectories, a problem that will be the subject of future investigation.

Declarations

Funding

The author L. P. P. is grateful for the financial support provided by CAPES Foundation (Coordination for the Improvement of Higher Education Personnel) during part of the development of this work. The work of M.V.F. and R.R-Jr was supported in part by the Dirección de Fomento de la Investigación at the PUCP through grant DFI-2025-PI1277. R.R-Jr was also supported in part by the National Council Scientific and Technological Development (CNPq) under Chamada CNPq/MCTI/No 10/2023-Universal. T.G. gratefully acknowledges the support of the London Mathematical Society with reference 42432 for sponsoring the visit of R.R. Jr. to the University of Essex, which made this work possible. T.G. would also like to thank the QJMAM Fund for Applied Mathematics for supporting the collaborative visit of M. V. F. to the University of Essex.

Author contributions

L.P.P, M.V.F, T.G and R.R-Jr: Conceptualization, Methodology, Investigation, Reviewing. L.P.P: Writing.

Conflict of interest

The authors state that there is no conflict of interest.

Data availability

Data sharing is not applicable to this article as all parameters used in the numerical experiments are informed in this paper.

References

[1] Abrashkin, A. A., Pelinovsky, E. N.: On the relation between Stokes drift and the Gerstner wave. Physics-Uspekhi **61**, 307–312 (2018). https://doi.org/10.3367/ufne.2017.03.038089

[2] Alfatih, A., Kalisch, H.: Reconstruction of the pressure in long-wave models with constant vorticity. Eur. J. Mech. B Fluids **37**, 187–194 (2013). https://doi.org/10.1016/j.euromechflu.2012.09.009

[3] Bakhoday-Paskyabi, M.: Particle motions beneath irrotational water waves. Ocean Dynamics **65**, 1063–1078 (2015). https://doi.org/10.1007/s10236-015-0856-4

[4] Bjørnestad, M., Grue, J., Jensen, A., Lagrangian measurements of orbital velocities in the surf zone. *Geophysical Research Letters* **48**(21), e2021GL095722 (2021). https://doi.org/10.1029/2021GL095722

[5] Borluk, H., Kalisch, H.: Particle dynamics in the KdV approximation. Wave Motion **49**, 691–709 (2012). https://doi.org/10.1016/j.wavemoti.2012.07.004

[6] Carter, J. D., Curtis, C. W., Kalisch, H.: Particle Trajectories in Nonlinear SchrÃűdinger Models. Water Waves **2**, 31–57 (2019). https://doi.org/10.1007/s42286-019-00008-7

[7] Chen, X., Cheng, J., Yin, X.: Advances and applications of electrohydrodynamics. Chin. Sci. Bull. **48**, 1055–1063 (2003). https://doi.org/10.1007/BF03185753

[8] Constantin, A.: The trajectories of particles in Stokes waves. Invent. Math. **166**, 523–535 (2006). https://doi.org/10.1007/s00222-006-0002-5

[9] Constantin, A., Villari, G.: Particle trajectories in linear water waves. J. Math. Fluid Mech. **10**, 1–18 (2008). https://doi.org/10.1007/s00021-005-0214-2

[10] Constantin, A., Strauss, W.: Pressure beneath a Stokes wave. Comm. Pure Appl. Math. **63**, 533–557 (2010). https://doi.org/10.1002/cpa.20299

[11] Constantin, O.: A complex-analytic approach to kinetic energy properties of irrotational traveling water waves. Mathematische Zeitschrift **301**, 4201–4215 (2022). https://doi.org/10.1007/s00209-022-03042-3

[12] Constantin, O.: A complex-analytic approach to streamline properties of deep-water Stokes waves. Arkiv för Matematik **61**, 81–97 (2023). https://dx.doi.org/10.4310/ARKIV.2023.v61.n1.a5

[13] Doak, A., Gao, T., Vanden-Broeck, J. M., Kandola, J. J. S.: Capillary-gravity waves on the interface of two dielectric fluid layers under normal electric fields. Quart. J. Mech. Appl. Math. **73**, 231–250 (2020). https://doi.org/10.1093/qjmam/hbaa009

[14] Doak, A., Gao, T., Vanden-Broeck, J.-M.: Global bifurcation of capillary-gravity dark solitary waves on the surface of a conducting fluid under normal electric fields. Quart. J. Mech. Appl. Math. **75**, 215–234 (2022). https://doi.org/10.1093/qjmam/hbac007

[15] Dyachenko, A.I., Kuznetsov, E.A., Spector, M., Zakharov, V.E.: Analytical description of the free surface dynamics of an ideal fluid (canonical formalism and conformal mapping). Phys. Lett. A **221**, 73–79 (1996). https://doi.org/10.1016/0375-9601(96)00417-3

[16] Easwaran, C.: Solitary waves on a conducting fluid layer. Phys. Fluids **31**, 3442–3443 (1988). https://doi.org/10.1063/1.866909

[17] Flamarion, M. V., Gao, T., Ribeiro-Jr, R., Doak, A.: Flow structure beneath periodic waves with constant vorticity under normal electric fields. Physics of Fluids **34**, 127119 (2022). https://doi.org/10.1063/5.0131563

[18] Flamarion, M. V.: Complex flow structures beneath rotational depression solitary waves in gravity-capillary flows. Wave Motion **117**, 103108 (2023). https://doi.org/10.1016/j.wavemoti.2022.103108

[19] Flamarion, M. V.: Flow patterns induced by a moving disturbance in rotational flows within the forced Korteweg–de Vries equation. Comput Appl Math. **43**, 446 (2024). https://doi.org/10.1007/s40314-024-02944-8

[20] Flamarion, M. V., Kochurin, E., Ribeiro-Jr, R.: Fully nonlinear evolution of free-surface waves with constant vorticity under horizontal electric fields. Mathematics **11**, 4467 (2023). https://doi.org/10.3390/math11214467

[21] Flamarion, M. V., Gao, T., Ribeiro-Jr, R.: An investigation of the flow structure beneath solitary waves with constant vorticity on a conducting fluid under normal electric fields. Physics of Fluids **35**, 037122 (2023). https://doi.org/10.1063/5.0142779

[22] Gao, T., Milewski, P. A., Papageorgiou, D. T., Vanden-Broeck, J.-M.: Dynamics of fully nonlinear capillary-gravity solitary waves under normal electric fields. J. Eng. Math. **108**, 107–122 (2018). https://doi.org/10.1007/s10665-017-9912-z

[23] Gao, T., Doak, A., Vanden-Broeck, J.-M., Wang, Z.: Capillary-gravity waves on a dielectric fluid of finite depth under normal electric field. Eur. J. Mech. B **77**, 98–107 (2019). https://doi.org/10.1016/j.euromechflu.2019.04.007

[24] Ghoshal, U., Miner A. C.: Cooling of high power density devices by electrically conducting fluids. U.S. Patent 6,658,861 (2003).

[25] Gleeson, H., Hammerton, P., Papageorgiou, D., Vanden-Broeck, J.-M.: A new application of the Korteweg-de Vries Benjamin-Ono equation in interfacial electrohydrodynamics. Phys. Fluids **19**, 031703 (2007). https://doi.org/10.1063/1.2716763

[26] Green, G.: On the motion of waves in a variable canal of small depth and width. Trans. of the Cambridge Phil. Soc. **6**, 457–462 (1838).

[27] Griffing, E. M., Bankoff, S. G., Miksis, M. J., Schluter R. A.: Electrohydrodynamics of thin flowing films. J. Fluids Eng. **128**, 276–283 (2006). https://doi.org/10.1115/1.2169811

[28] Grue, J., Kolaas, J., Jensen, A.: Experimental particle paths and drift velocity in steep waves at finite water depth. *Journal of Fluid Mechanics* 810, R1 (2017) https://doi.org/10.1017/jfm.2016.726.

[29] Guyenne P, Kalisch H. Impact of mean water level on particle drift in shallow and intermediate depth. *Journal of Fluid Mechanics.* 2025;1020:A22. doi:10.1017/jfm.2025.10666

[30] Hammerton, P.: Existence of solitary travelling waves in interfacial electrohydrodynamics. Wave Motion **50**, 676–686 (2013). https://doi.org/10.1016/j.wavemoti.2013.01.003

[31] Hunt, M. J., Vanden-Broeck, J.-M.: A study of the effects of electric field on two-dimensional inviscid nonlinear free surface flows generated by moving disturbances. J. Eng. Math. **92**, 1–13 (2015). https://doi.org/10.1007/s10665-014-9766-6

[32] Khorsand, Z.: Particle trajectories in the Serre equations. Appl. Math. Comput. **230**, 35–42 (2014). https://doi.org/10.1016/j.amc.2013.12.018

[33] Kistler, S. F., Schweizer, P. M.: Liquid Film Coating - Scientific Principles and their Technological Implications. Chapman and Hall, Springer, New York (1997).

[34] Li, J., Yang, S.: Kinetic energy properties of irrotational deep-water Stokes waves. arXiv preprint (2024). https://arxiv.org/abs/2406.00711

[35] Longuet-Higgins, M. S: Mass transport in water waves, Philosophical Transactions of the Royal Society of London. Series A, Mathematical and Physical Sciences, **245**, 535-581 (1953).

[36] Longuet-Higgins, M. S.: The trajectories of particles in steep, symmetric gravity. J. Fluid Mech. **94**, 497–517 (1979). https://doi.org/10.1017/S0022112079001154

[37] Longuet-Higgins, M. S.: Eulerian and Lagrangian aspects of surface waves. J. Fluid Mech. **173**, 683–707 (1986). https://doi.org/10.1017/S0022112086001325

[38] Melcher, J. R., Schwarz, W.J.: Interfacial relaxation overstability in a tangential electric field. Phys. Fluids **11**, 2604–2616 (1968). https://doi.org/10.1063/1.1691866

[39] Moulton, D. E., Pelesko, J. A.: Catenoid in an electric field. SIAM J. Appl. Math. **70**, 212–230 (2009). https://doi.org/10.1137/070698579

[40] Nachbin, A., Ribeiro-Jr, R.: A boundary integral formulation for particle trajectories in stokes wave. Disc. and Cont. Dynamical Systems **34**, 3135–3153 (2014). https://doi.org/10.3934/dcds.2014.34.3135

[41] Nachbin, A., Ribeiro-Junior, R.: Capturing the flow beneath water waves. Phil. Trans. R. Soc. A **376**, 20170098 (2018). https://doi.org/10.1098/rsta.2017.0098

[42] Papageorgiou, D. T., Vanden-Broeck, J.-M.: Numerical and analytical studies of nonlinear gravity-capillary waves in fluid layers under normal electric fields. IMA J. Appl. Math. **72**, 832–853 (2006). http://dx.doi.org/10.1093/imamat/hxm040

[43] Papageorgiou, D. T.: Film flows in the presence of electric fields. Ann. Rev. Fluid Mech. **51**, 155–187 (2019). http://dx.doi.org/10.1146/annurev-fluid-122316-044531

[44] Perelman, T., Fridman, A., Eliashevich, M.: Modified Korteweg-de Vries equation in electrohydrodynamics. Sov. Phys. JETP **39**, 643–646 (1974).

[45] Ribeiro-Jr, R., Milewski, P. A., Nachbin, A.: Flow structure beneath rotational water waves with stagnation points. J. Fluid Mech. **812**, 792–814 (2017). https://doi.org/10.1017/jfm.2016.820

[46] Stokes, G. G.: On the theory of oscillatory waves. Trans. Cambridge Phil. Soc. **8**, 441–455 (1847).

[47] Taylor, G., McEwan, A.: The stability of a horizontal fluid interface in a vertical electric field. J. Fluid Mech. **22**, 1–15 (1965). https://doi.org/10.1017/S0022112065000538

[48] Taylor, G. I., Van Dyke, M. D.: Electrically driven jets. Proc. R. Soc. A **313**, 453–475 (1969). https://doi.org/10.1098/rspa.1969.0205

[49] Ursell, F.: Mass transport in gravity waves. Proc. Cambridge Phil. Soc. **49**, 145–150 (1953). https://doi.org/10.1017/S0305004100028140

[50] van den Bremer, T. S., Breivik, ø.: Stokes Drift. Phil. Trans. of the R.S A: Math., Phys. and Eng. Sciences **376**, 20170104 (2017). https://doi.org/10.1098/rsta.2017.0104

[51] Vanneste, J., Young, W. R.: Stokes drift and its discontents. Phil. Trans. R. Soc. A **380**, 20210032 (2022). https://doi.org/10.1098/rsta.2021.0032

[52] Wang, Z.: Modelling nonlinear electrohydrodynamic surface waves over three-dimensional conducting fluids. Proc. R. Soc. A **473**, 20160817 (2017). https://doi.org/10.1098/rspa.2016.0817

[53] Weber, J. E. H.: A Lagrangian study of internal Gerstner- and Stokes-type gravity waves. Wave Motion **88**, 257–264 (2019). https://doi.org/10.1016/j.wavemoti.2019.06.002

A Shallow and deep-Water regime

In this appendix, we aim to summarize the results obtained for waves in the shallow-water and deep-water regimes. We consider $\lambda_S = 10\pi$ and $\lambda_D = 0.5$ as wave length for shallow-water and deep-water regime, respectively. The same numerical methods previously applied to intermediate-water wave ($\lambda = 2\pi$) regimes were used, and we investigated the variation of the drift time τ with E_b variation, as well the geometric parameters of the orbit and the total kinetic energy of the particles.

Our numerical experiments show analogous results for waves in intermediate-water regime. The drift time τ as function of the eletric Bond number E_b is crescent, as we can see in Figure 12. Table 1 shows the order of the relative deviation of the trajectory parameters d_1, d_2 and d_3 with respect to the reference case $E_b = 0$ in both regimes. The order of the relative deviation for the intermediate water wave regime is additionally presented in this table as a scale for comparison.

	$E_r(d_1)$	$E_r(d_2)$	$E_r(d_3)$
Shallow-water	10^{-6}	10^{-10}	10^{-8}
Intermediate-water	10^{-10}	10^{-6}	10^{-6}
Deep-water	10^{-6}	10^{-10}	10^{-10}

Table 1: Order of the relative errors in three different regimes.

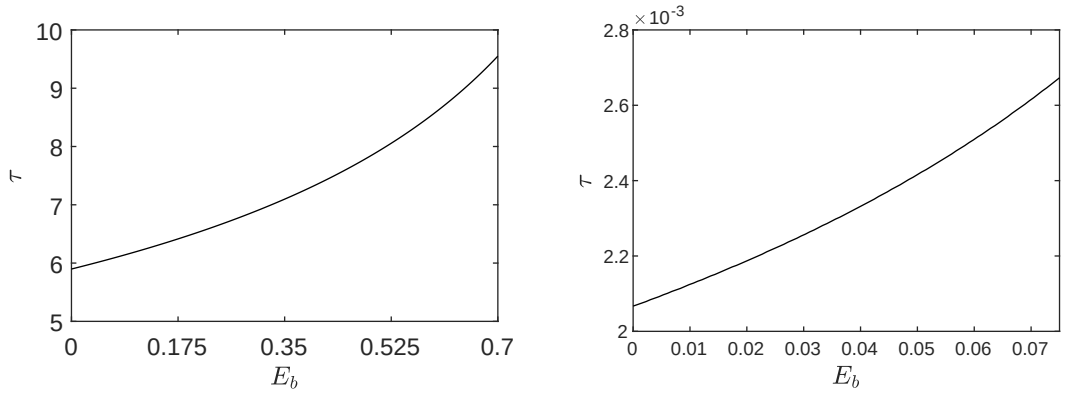

Figure 12: Drift time in function of E_b. Left: Shallow-water regime. Right: Deep-water regime.

For the total kinetic energy of the particles, our results are presented in Figure 13 for shallow and deep-water regimes. As we can see in these figure, in fixed frame $\mathcal{E}(X_0, Y_0)$ is a convex and non-decreasing function and in moving frame $E(X_0, Y_0)$ is a constant function equal to $c\lambda/2$. Furthermore, the total kinetic energy of the particles in both regimes and frames of reference is lower for stronger electric fields.

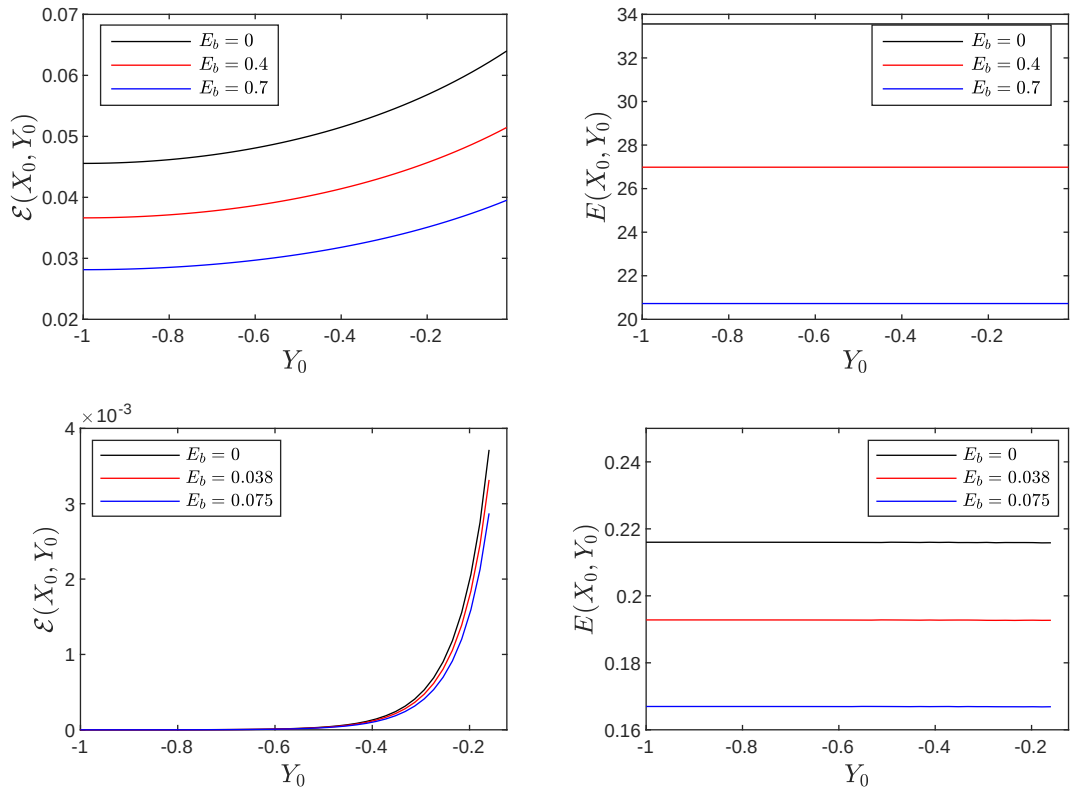

Figure 13: Total kinetic energy of particles as a function of the particle's initial depth (Y_0) for different values of E_b. Up: Shallow-water regime. Down: Deep-water regime Left: Fixed frame. Right: Moving frame.

B Reparametrization of the ODEs for Particle Trajectories

For completeness, we provide here a detailed explanation showing why the shape of the particle trajectories is unaffected by the electric Bond number E_b. We show that variations in E_b only correspond to a reparameterization of the trajectories.

From equation (28), the potential can be written as

$$\begin{aligned}\tilde{\phi}(\xi,\zeta) &= \mathcal{F}^{-1}_{k\neq 0}\left[\frac{\cosh(k_j(D+\zeta))}{\cosh(k_j D)}\hat{\mathbf{\Phi}}(k)\right] \\ &= -c\,\mathcal{F}^{-1}_{k\neq 0}\left[\frac{\cosh(k_j(D+\zeta))}{\cosh(k_j D)}\, i\coth(k_j D)\hat{\mathbf{Y}}(k_j)\right]\end{aligned} \tag{32}$$

This implies that:

$$\tilde{\phi}_\xi(\xi,\zeta) = -c\mathcal{L}(\mathbf{Y}(\xi),\zeta)) \tag{33}$$

$$\tilde{\phi}_\zeta(\xi,\zeta) = -c\mathcal{M}(\mathbf{Y}(\xi),\zeta)) \tag{34}$$

where

$$\mathcal{L}(\mathbf{Y}(\xi),\zeta)) := -\mathcal{F}^{-1}_{k\neq 0}\left[\frac{\cosh(k_j(D+\zeta))}{\cosh(k_jD)}\,\coth(k_jD)k_j\hat{\mathbf{Y}}(k_j)\right],$$

$$\mathcal{M}(\mathbf{Y}(\xi),\zeta)) := \mathcal{F}^{-1}_{k\neq 0}\left[\frac{k_j\sinh(k_j(D+\zeta))}{\cosh(k_jD)}\,i\coth(k_jD)\hat{\mathbf{Y}}(k_j)\right].$$

Substituting (33) and (34) into (27), we obtain

$$\begin{cases}\dfrac{1}{c}\dfrac{d\xi}{dt} = -\dfrac{1}{J}\left(\mathcal{L}+\tilde{Y}_\zeta\right),\\[2ex] \dfrac{1}{c}\dfrac{d\zeta}{dt} = -\dfrac{1}{J}\left(\mathcal{M}-\tilde{Y}_\xi\right).\end{cases} \tag{35}$$

Note that $\mathcal{L}$ and $\mathcal{M}$ do not depend on E_b. As shown in equation (23), for an electrified periodic wave with profile $\mathbf{Y}$ (depth D) and speed c, the profile coincides with that of a classical Stokes wave with speed

$$c_s^2 = c^2 + \frac{E_b}{D^2}.$$

If we now introduce the new parameter $\theta = ct$, then system (35) is reparametrized in terms of θ instead of t. The trajectories $(\xi(t),\zeta(t))$ remain exactly the same curves in the (ξ,ζ)-plane; the effect of changing E_b is only to modify the parametrization speed along these trajectories.

Therefore, the presence of the electric field does not alter the shape of the particle paths. It only changes the rate at which the particles move along them.